ADVANCES IN ATMOSPHERIC SCIENCES, VOL. 36, JANUARY 2019, 65–78

• **Original Paper** •

A Numerical Study of Mesoscale Vortex Formation in the Midlatitudes: The Role of Moist Processes

Yongqiang JIANG[1,2], Yuan WANG[*1], Chaohui CHEN[2], Hongrang HE[2], and Hong HUANG[1,2]

[1] *Key Laboratory of Mesoscale Severe Weather/Ministry of Education of China, and School of Atmospheric Sciences, Nanjing University, Nanjing* 210093*, China*

[2] *Institute of Meteorology and Oceanography, National University of Defense Technology, Nanjing* 211101*, China*

(Received 19 December 2017; revised 16 May 2018; accepted 31 July 2018)

ABSTRACT

In this study, a three-dimensional mesoscale model was used to numerically simulate the well-known "98.7" heavy rainfall event that affected the Yangtze Valley in July 1998. Two experiments were conducted to analyze the impact of moist processes on the development of meso-β scale vortices (MβV) and their triggering by mesoscale wind perturbation (MWP). In the experiment in which the latent heat feedback (LHF) scheme was switched off, a stable low-level col field (i.e., saddle field—a region between two lows and two highs in the isobaric surface) formed, and the MWP triggered a weak MβV. However, when the LHF scheme was switched on as the MWP was introduced into the model, the MβV developed quickly and intense rainfall and a mesoscale low-level jet (mLLJ) were generated. The thickness of the air column and average temperature between 400 and 700 hPa decreased without the feedback of latent heat, whereas they increased quickly when the LHF scheme was switched on, with the air pressure falling at low levels but rising at upper levels. A schematic representation of the positive feedbacks among the mesoscale vortex, rainfall, and mLLJ shows that in the initial stage of the MβV, the MWP triggers light rainfall and the latent heat occurs at low levels, which leads to weak convergence and ageostrophic winds. In the mature stage of the MβV, convection extends to the middle-to-upper levels, resulting in an increase in the average temperature and a stretching of the air column. A low-level cyclonic circulation forms under the effect of Coriolis torque, and the mLLJ forms to the southeast of the MβV.

Key words: moist process, latent heat feedback, mesoscale vortex, col field

Citation: Jiang, Y. Q., Y. Wang, C. H. Chen, H. R. He, and H. Huang, 2019: A Numerical study of mesoscale vortex formation in the midlatitudes: the role of moist processes. *Adv. Atmos. Sci.*, **36**(1), 65–78, https://doi.org/10.1007/s00376-018-7234-3.

1. Introduction

Mesoscale vortices are one of the most important weather systems associated with heavy rainfall. During the summer in China, an approximately west–east orientated 850- or 700-hPa shear line associated with the mei-yu front usually occurs over the Yangtze River basin. Ninomiya (2000) indicated that the meso-α-scale mei-yu front is characterized by intense precipitation, a low-level jet (LLJ) stream, nearly moist-neutral stratification, and a strong gradient of equivalent potential temperature. Ninomiya (2000) also showed that the strong latent heat release (LHR) is one of the factors that sustains the ascending motion in the frontal zone. Studies have shown that many mesoscale low-level vortices form within the shear line, and the LLJ to the south of the shear line brings warm and moist air to the heavy rainfall regions (Matsumoto et al., 1970; Ding, 1992; Chen et al., 2006). Matsumoto et al. (1970) referred to the low-level low within the mei-yu front as an intermediate-scale (300–1000 km) system that forms under the synoptic-scale background. With the development of observational techniques and mesoscale models, high-spatial-resolution data analysis (Bei et al., 2002; Wang et al., 2003; Xu et al., 2011; Jiang and Wang, 2012) has shown that large numbers of low-level systems that directly induce heavy rainfall are meso-α- or meso-β-scale vortices (MβVs) with size scales of several hundred kilometers in midlatitude China.

The moist processes, and in particular LHR, are essential for the development of cyclones and intensification of the associated rainfall (Kuo and Reed, 1988; Davis, 1992; Stoelinga, 1996; Novak et al., 2009; Xu et al., 2011). By using mesoscale reanalysis data, Xu et al. (2011) indicated that the evolution of mesoscale convective vortices is closely related to the strength of the positive interaction between convection and the vortex. Posselt and Martin (2004) showed

* Corresponding author: Yuan WANG
Email: yuanasm@nju.edu.cn

that LHR associated with precipitation poleward of the surface low enhances the development of the potential vorticity (PV) treble-cleft structure aloft. Using two-dimensional numerical integrations, Cho (1993) indicated that the mesoscale organization of precipitation in midlatitude cyclones may be caused by a positive feedback process between potential-vorticity anomalies and LHR during condensation.

Previous studies have demonstrated that the development of a mesoscale low-level vortex is associated with the intensification of the LLJ to the south of a heavy rainfall region, which is driven by the downward mixing of southwesterly momentum from upper levels by convection (Ninomiya and Akiyama, 1974), the adjustment of the thermal wind (Chen, 1982), the interaction between the upper-level jet and adiabatic processes (Uccellini et al., 1987), and the feedback of latent heat from precipitation (Hsu and Sun, 1994; Chen et al., 2006). Chen et al. (1998) indicated that the heavy rainfall associated with the mei-yu front over the Yangtze basin is triggered by a perturbation that is caused by a mesoscale LLJ (mLLJ). The intense rainfall and mLLJ develop simultaneously, and there is a positive relationship between heavy rainfall and the mLLJ. They also indicated that the relationship between heavy rainfall and the mLLJ remains unclear. Using a numerical simulation of a mesoscale convective system (MCS) that generated heavy rainfall over Taiwan on 7 June 1998, Zhang et al. (2003b) found that the pressure gradient force and the horizontal advection were the main contributors to the development of the mLLJ in the developing stage. However, the role of moist processes in the development of the mLLJ and mesoscale vortices in the aforementioned studies left many questions to be answered.

Why do many mesoscale low-level vortices form within the shear line? What roles does the mLLJ to the south of the shear line play in the formation of vortices? What is the relationship between the mLLJ, LHR and vortices? One of the difficulties associated with studying the role of moist processes within mesoscale vortices is to separately evaluate the effects of the thermal and dynamic processes and the feedback of thermal effects to the wind fields. However, although it is important to isolate the effects of the thermal and dynamic processes, it is difficult to trigger the mesoscale vortex using dynamic processes when the thermal process scheme is switched off in the model. Our research (Jiang and Wang, 2012; Jiang et al., 2012) has demonstrated that a weak wind environment favors the formation of mesoscale vortices. A weak mesoscale vortex can be triggered by mesoscale wind perturbation (MWP) in the col field (i.e., saddle field—a region between two lows and two highs in the isobaric surface). In this paper, the famous "98.7" heavy rainfall event that occurred in eastern Hubei Province (Bei et al., 2002), which was a typical case of heavy rainfall developing in a steady col field, is studied numerically using an improved version of the three-dimensional η-coordinate mesoscale model designed by Yu et al. (1994). In an idealized experiment, an MWP is induced in the col field in the model without considering the thermal effects. For comparison, another idealized experiment, which included the thermal effects, is analyzed to study the role of moist processes in mesoscale vortices.

2. Model and method

We used the same model for this study as did Jiang and Wang (2012). The model is an improved version of the three-dimensional η-coordinate mesoscale model designed by Yu et al. (1994). The experiments were performed using the domain (20°–50°N, 70°–125°E), with a horizontal resolution of $0.25° \times 0.125°$ in the zonal and meridional directions, respectively, and 23 vertical levels. The simulation settings included the cumulus parameterization Betts (1986) and the Blackada planetary boundary layer parameterization (Zhang and Anthes, 1982).

In Jiang and Wang (2012), an MWP was introduced into the model near the col point (a singular point in the col field where the wind speed is zero), and the perturbation-induced MβV was analyzed. It was shown that the MβV induced by the MWP was weak and persisted for only a few hours if the latent heat feedback (LHF) scheme was switched off in the model. The magnitude of the MWP also decreased rapidly. However, when the model LHF scheme was switched on, the mLLJ and MβV developed rapidly and were accompanied by intense rainfall. For this study, we conducted two experiments to investigate the effects of LHF on MβV development. The perturbation wind is defined as:

$$u' = U_0 e^{-cr^2}, \quad v' = V_0 e^{-cr^2}, \tag{1}$$

where r is the distance apart from the perturbation center, c is the attenuation coefficient of the wind speed, and U_0 and V_0 are the central wind speed of perturbation in the x- and y-direction, respectively. The central wind speed of initial southwesterly MWP, located at (31°N, 114.25°E), was set as 25 m s^{-1}. The MWP with the same structure at 8–17 model levels (about 600 to 850 hPa) was prescribed.

In this study, the LHF was taken to be the main element of the moist processes. The numerical experiment scheme is shown in Table 1. In EXP1, the LHF scheme was switched off for the whole run, whereas in EXP2 it was switched on as the perturbation was introduced into the model at t = 17 h. In the control simulations (i.e., real simulations, considering the LHF but without MWP), the 700-hPa mLLJ to the south of the col point that occurs at t = 17 h intensifies with the integration. The maximum wind speed of the mLLJ was greater than 12 m s^{-1} at t = 24 h in association with the intensification of the MβV and rainfall (figures omitted). Without considering the LHF, the mLLJ and MβV cannot form, so the MWP was introduced into the model at t = 17 h.

Table 1. Numerical experimental design.

Experiment	LHF
EXP1	Switched off
EXP2	Switched on as the perturbation is introduced into the model

3. Numerical experiments

3.1. *Description of the "98.7" heavy rainfall event in China*

The "98.7" heavy rainfall event is well known all over China. During 21–22 July 1998, heavy rainfall fell along the Yangtze River Valley in eastern Hubei Province. The accumulated precipitation was 633 mm at the Parrot Island station in Wuhan, and 501.8 mm of rain fell in Huangshi over the two days, leading to serious flooding across the Yangtze basin. It has been suggested that this heavy rainfall was directly triggered by a meso-β scale weather system (Bei et al., 2002; Jiang and Wang, 2012).

Figure 1 shows the 500-hPa synoptic map and 700-hPa streamlines at 0000 UTC 21 July 1998 based on the 0.5° × 0.5° resolution GAME (GEWEX Asian Monsoon Experiment; GEWEX: Global Energy and Water Cycle Experiment) reanalysis data provided by the Japan Meteorological Agency and the Earth Observation Research Center/National Space of Development Agency of Japan. The precipitation dataset was obtained from the National Meteorological Center of China. The southwest vortex (SWV), which was located over (26°–32°N, 102°–112°E), was so strong that it is very clear at 500 hPa. Wuhan was located to the east of the SWV, where the winds were relatively light. A col field is evident between the SWV and the vortex in Anhui Province at 700 hPa, and Wuhan is close to the col point. The southwest flows to the south of the col field brought warm and moist air to the region of heavy rainfall.

3.2. *EXP1*

Figure 2 shows the evolution of the 700-hPa streamlines and vorticity in EXP1 and EXP2. In EXP1, the MWPs induce a mesoscale positive vertical relative vorticity (hereafter, vorticity) region with a maximum vorticity greater than 16×10^{-5} s^{-1}near the col point at t = 17 h. The maximum vorticity then falls rapidly to about 8×10^{-5} s^{-1} at t = 19 h, and to about 4×10^{-5} s^{-1} at t = 21 h. The vorticity is then maintained at the same intensity until t = 27 h, but the maximum value falls to less than 4×10^{-5} s^{-1} at t = 30 h. Under the influence of MWPs, a dynamic MβV forms near the col point at t = 21 h. The MβV is so weak that it persists for less than 2 h. This suggests that MWPs are able to induce a weak MβV. However, the MβV is short-lived without the LHF.

3.3. *EXP2*

As in EXP1, the positive vorticity also decreases quickly as the perturbation is introduced into the model (Figs. 2d–f). The maximum vorticity fell to about 8×10^{-5} s^{-1} at t = 19 h because of the weak rainfall and associated weak LHR before t = 19 h. Figure 3 shows the evolution of precipitation intensity within (30°–31°N, 113.5°–114.5°E) in EXP1 and EXP2. The region covers the 48-h accumulated precipitation center near Wuhan in EXP2. The precipitation amount is extremely small in EXP1 (without LHF), whereas it increases rapidly after the LHF scheme is switched on in EXP2. With the intensification of the rainfall in EXP2, the vorticity increases after t = 21 h. The MβV forms at t = 19 h, which is earlier than in EXP1 by about 2 h. When the rainfall intensifies, the MβV also develops, with a maximum vorticity greater than 12×10^{-5} s^{-1} at t = 21 h and 20×10^{-5} s^{-1} at t = 23 h. Our simulation results show that the LHF must play an important role in the development of the MβV.

Figure 4 shows the evolution of the 700-hPa winds, vorticity, divergence, and 2.5-min accumulated precipitation in EXP2. The southwesterly MWPs result in the formation of the vorticity and a divergence couplet. The vorticity maintains its intensity until t = 30 min, with a maximum vorticity greater than 12×10^{-5} s^{-1}. This vorticity is the source of the weak MβV formation. Although the divergence couplet decreases rapidly, it triggers the deep mesoscale vertical circulation (not shown). There are two inverse circulations above

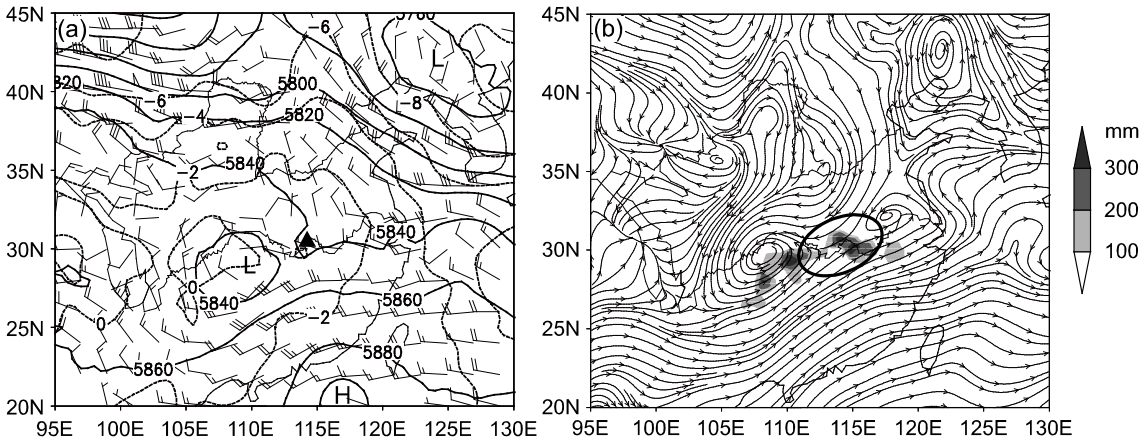

Fig. 1. Synoptic maps from (a) 500 hPa and (b) 700 hPa at 0000 UTC 21 July 1998. The solid lines denote geopotential height (contoured every 20 gpm); the dashed lines denote temperature (contoured every 2°C); full and half barbs represent 4 and 2 m s^{-1}, respectively; the solid lines with arrows denote streamlines; the shading shows the 48-h accumulated precipitation (mm) from 0000 UTC 21 to 0000 UTC 23 July 1998; "▲" marks the location of Wuhan in Hubei Province; and the ellipse frame denotes the 700-hPa col field.

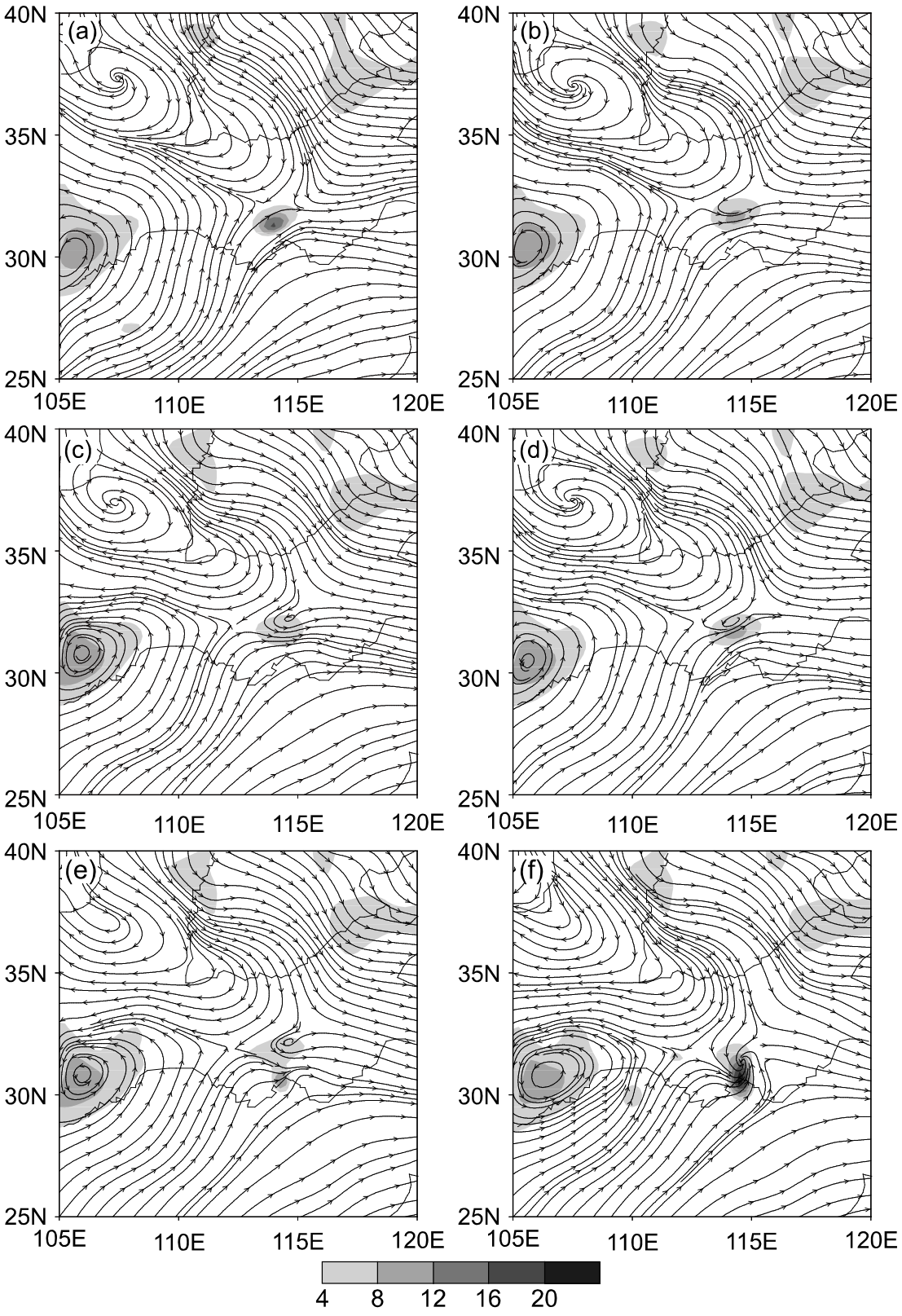

Fig. 2. 700-hPa streamlines and vorticity (units: 10^{-5} s^{-1}) in EXP1 at (a) t = 17 h, (b) t = 19 h and (c) t = 21 h, and in EXP2 at (d) t = 19 h, (e) t = 21 h and (f) t = 23 h. The shading denotes vorticity greater than 4×10^{-5} s^{-1}.

and below 800 hPa. The 2.5-min accumulated precipitation patterns show that the rainfall occurs mainly in the 700-hPa divergence region, but not in the convergence region. The water vapors transported by the southwesterly flows condense after being lifted by the updrafts associated with the shallow vertical circulation below 800 hPa.

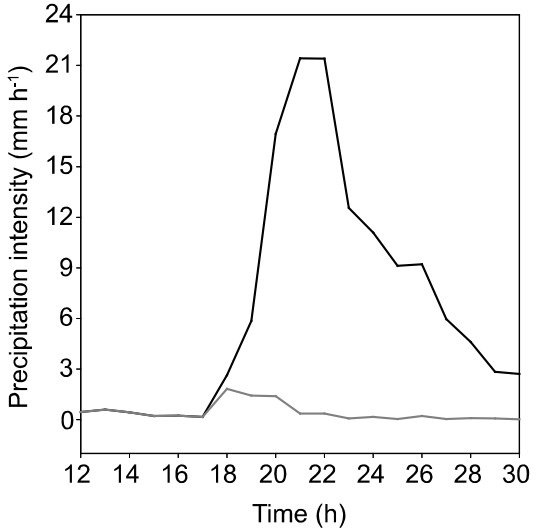

Fig. 3. Evolution of average precipitation intensity (mm h^{-1}) in region of 30°–31°N, 113.5°–114.5°E in EXP1 (gray line) and EXP2 (black line).

3.4. *Comparative analysis*

Figure 5 shows the differences in the 700-hPa wind speed and geopotential height between EXP2 and EXP1. After 1 h of integration (i.e., t = 18 h) as the MWP is introduced into the model, the wind speed near the perturbation in EXP2 is slightly greater than that in EXP1. The maximum difference is about 0.6 m s^{-1}. However, the geopotential height near the perturbation in EXP2 is greater than that in EXP1, with a maximum difference greater than 4 gpm. With the intensification of rainfall in EXP2, the latent heat increases. An MβV forms to the northwest of the perturbation at t = 19 h. The wind speeds decrease near the vortex center and increase to the northeast and southwest of the vortex. The geopotential heights in EXP2 also decrease quickly near the vortex center, with a difference of less than −8 gpm at t = 20 h and less than −14 gpm at t = 24 h. The wind speeds to the south and north of the vortex in EXP2 increase with the integration, respectively. The maximum wind speed differences are greater than 2.5 m s^{-1} at t = 24 h and greater than 4 m s^{-1} at t = 30 h. As

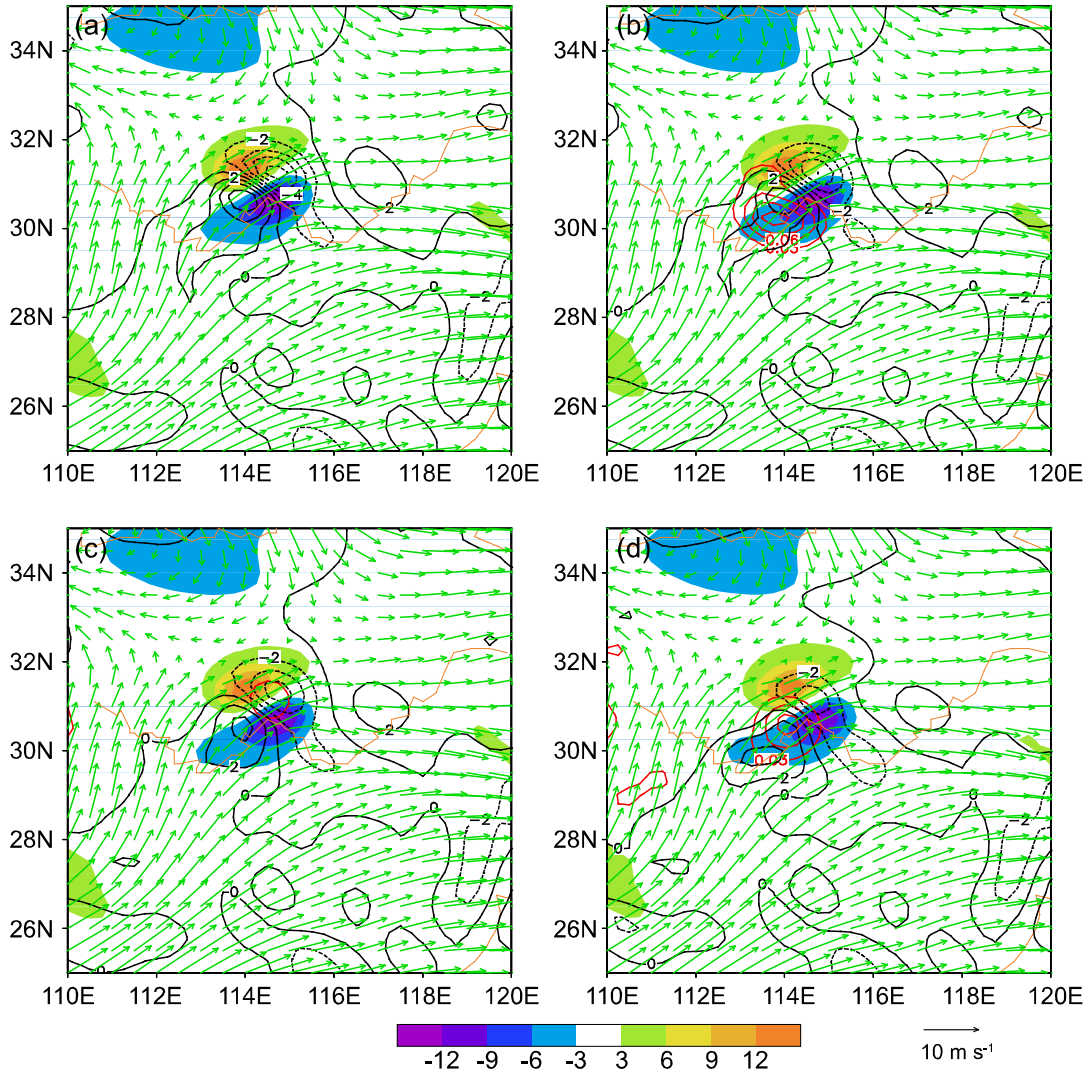

Fig. 4. 700-hPa vorticity (shaded; contoured every 3×10^{-5} s^{-1}), divergence (black lines; contoured every 2×10^{-5} s^{-1}), wind vectors (green arrows; units: m s^{-1}), and 2.5-min accumulated precipitation (red lines; every 0.03 mm), at (a) 0 min, (b) 5 min, (c) 10 min and (d) 30 min, from t = 17 h, in EXP2.

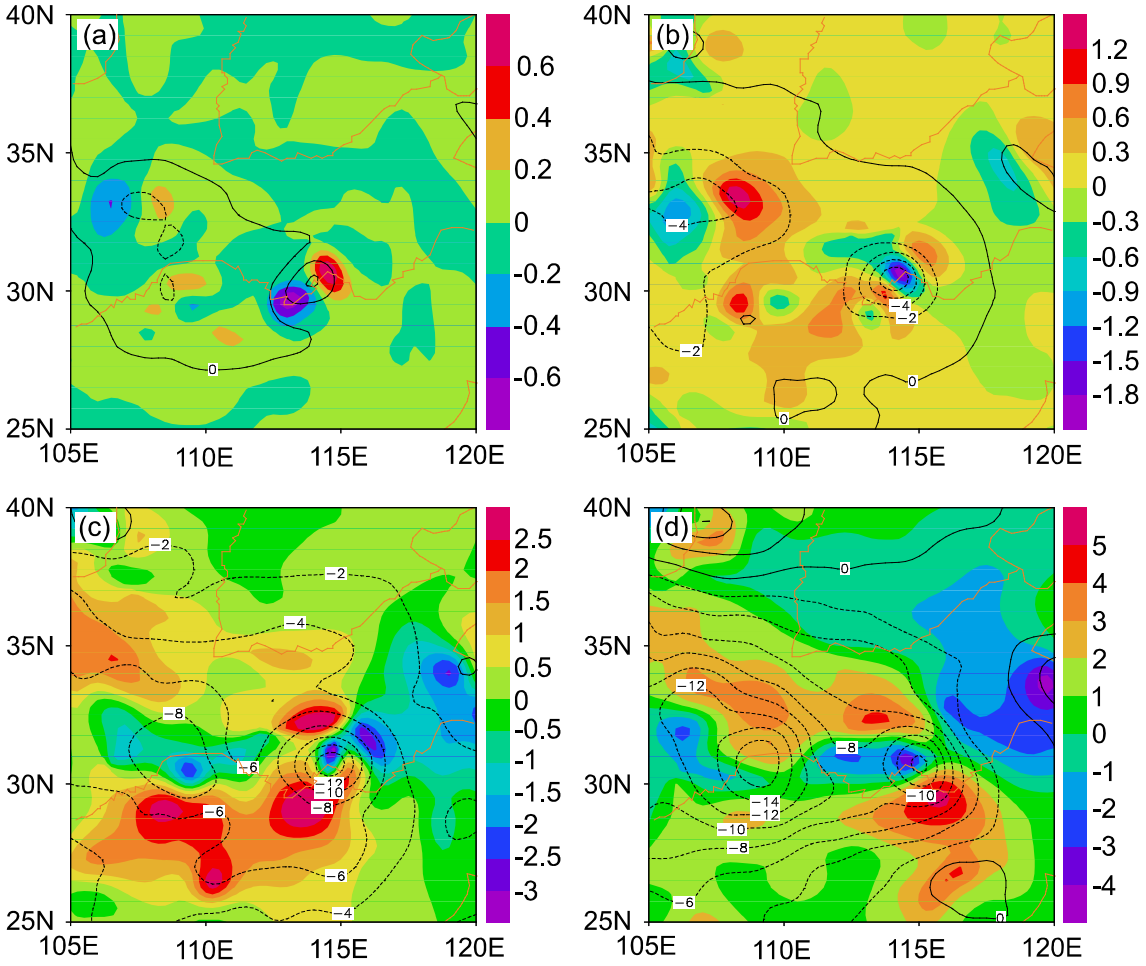

Fig. 5. Differences in 700-hPa wind speed (shaded according to scale; units: m s^{-1}) and geopotential height (lines; contoured every 2 gpm) between EXP2 and EXP1 at (a) t = 18 h, (b) t = 20 h, (c) t = 24 h and (d) t = 30 h.

the scale of the strong wind region is about 100 to 200 km, we follow Chen et al. (1998) and define it as an mLLJ. This mLLJ can be regarded as the mesoscale disturbance associated with the rainstorms in their study. Our simulation results suggest that the low-level pressure drops are caused by the LHR, and then the mLLJ intensifies and the MβV develops. The southwesterly and northeasterly mLLJs to the south and north of the MβV play important roles in the development of the MβV.

Figure 6 shows the differences in the 500-hPa wind speed and geopotential height between EXP2 and EXP1. The wind speeds above the perturbation in EXP2 increase clearly from t = 18 h to t = 20 h, while the wind speeds to the southwest of the perturbation decrease. A weak wind speed difference center forms above Wuhan at t = 24 h, along with a weak cyclonic circulation. At the same time, the wind speeds to the north and south of the weak vortex in EXP2 increase and decrease, respectively. The evolution of the 500-hPa geopotential height is markedly different from that at 700 hPa. Under the influence of the latent heat in EXP2, the 500-hPa geopotential height rises near the perturbation, leading to a difference greater than 10 gpm by t = 20 h.

According to hydrostatic balance theory, the thickness of the air column is proportional to average temperature,

$$\Delta z = \frac{R\overline{T}}{g_0} \ln \frac{p_b}{p_t} , \tag{2}$$

where p_b and p_t are the pressure of isobaric surfaces; Δz and $\overline{T}$ are the thickness and average temperature of the air column between p_b and p_t, respectively; R is the gas constant; and g_0 is the average of the gravitational acceleration. We define the thickness of the air column and average temperature between 400 and 700 hPa as DH and TA, respectively:

$$\mathrm{DH} = H_{400} - H_{700} ; \tag{3}$$

$$\mathrm{TA} = \frac{1}{\log p_6 - \log p_1} \sum_{n=2}^{5} T_n (\log p_{n+1} - \log p_{n-1}) . \tag{4}$$

Here, H is the geopotential height; T_n (n = 2...5) is the temperature at the 400, 500, 600 and 700 hPa levels; and p_n (n = 1...6) is the pressure at 300, 400, 500, 600, 700 and 800 hPa. Next, we define the differences in DH and TA between EXP2 and EXP1 as DDH and DTA:

$$\mathrm{DDH} = \mathrm{DH}_{\mathrm{EXP2}} - \mathrm{DH}_{\mathrm{EXP1}} ; \tag{5}$$

$$\mathrm{DTA} = \mathrm{TA}_{\mathrm{EXP2}} - \mathrm{TA}_{\mathrm{EXP1}} . \tag{6}$$

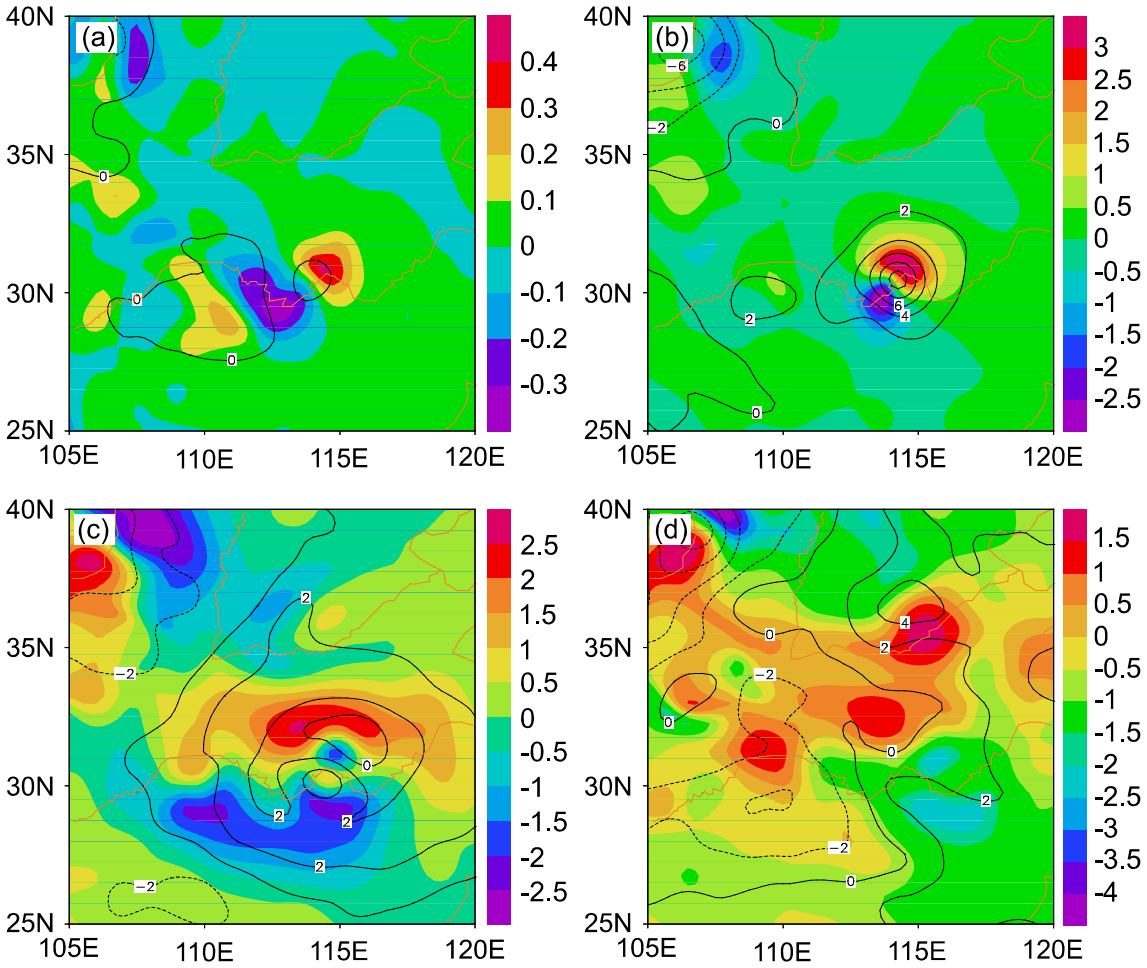

Fig. 6. As in Fig. 5 but at 500 hPa.

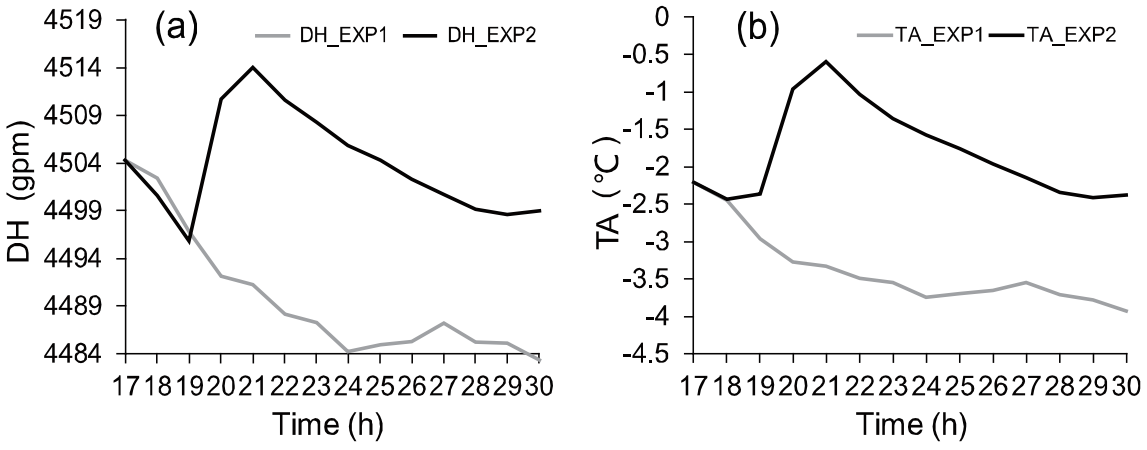

Fig. 7. Evolution of (a) average DH (units: gpm) and (b) average TA (units: °C) within (30°–31°N, 113.5°–114.5°E), where the rainfall was relatively intense, in EXP2. The gray line indicates EXP1 and the black line EXP2.

Figure 7 shows the evolution of average DH and average TA within (30°–31°N, 113.5°–114.5°E). The evolution of average DH is similar to that of average TA, because DH is directly proportional to TA under the hydrostatic balance constraint. In EXP1, average DH decreases from 4504.3 gpm at t = 17 h to 4484.2 gpm at t = 24 h, and varies little after that; whereas, in EXP2, average DH increases rapidly from about 4495.8 gpm at t = 19 h to about 4514.0 gpm at t = 21 h. During this period, the upper-level pressure rises and the low-level pressure drops, resulting in the increase in DH. The value of average TA in EXP2 rises by 2.7°C at t = 21 h compared with that in EXP1.

The horizontal cross sections of DDH and DTA are shown in Fig. 8. DDH is negative near the perturbation at t = 18 h, which corresponds to a weakly negative DTA center. The DDH intensifies quickly with the integration. The maximum DDH is greater than 21 gpm in association with a positive DTA center with a maximum DTA greater than 2.7°C at t = 20 h. The regions of positive DDH and DTA extend, whereas the intensities weaken with the integration before t = 24 h. By t = 30 h, the maximum values of DDH and DTA decrease to about 18 gpm and 1.6°C, respectively.

Figure 9 shows the horizontal cross section of the 700-hPa difference vorticity and wind between EXP2 and EXP1. Both the difference in vorticity and wind is very small at t = 18 h. The difference in vorticity increases in association with the intensification of the difference in wind. The maximum value of the difference in vorticity is greater than 3×10^{-5} s^{-1} near the perturbation at t = 20, and it increases rapidly after t = 21 h, with the maximum value being greater than 16×10^{-5} s^{-1} at t = 24 h. A mesoscale cyclonic circulation forms in the difference in the wind field at t = 21 h (not shown). By t = 30 h, the difference in vorticity is rather large, with the positive-value region and the cyclonic circulation extending to the meso-α scale. We also see that the regions of positive difference in vorticity all correspond to the cyclonic circulations, suggesting that the latent heating is responsible for the intensification of the MβV.

To analyze the energy difference between the two simulations, we defined the difference in the total energy (DTE) per unit mass (Zhang et al., 2003a; Tan et al., 2004) and total kinetic energy per unit mass. The DTE is expressed as

$$\mathrm{DTE} = \frac{1}{2}\sum(U'^2_{i,j,k} + V'^2_{i,j,k} + \kappa T'^2_{i,j,k}) \,, \tag{7}$$

where U', V' and T' are the differences in the wind components and the difference in temperature between EXP2 and EXP1; $\kappa = C_p/R$; i and j run over x and y grid points over the region (20°–50°N, 80°-120°E); and k runs over the 11 levels of 1000, 925, 850, 775, 700, 600, 500, 400, 300, 200 and 100 hPa. The total kinetic energy (TKE) per unit mass is defined as

$$\mathrm{TKE} = \frac{1}{2}\sum(U^2_{i,j,k} + V^2_{i,j,k} + W^2_{i,j,k}) \,, \tag{8}$$

where U and V are the x- and y-components of wind speed, respectively, and W is the vertical velocity in the z coordinate.

The evolution of the DTE is shown in Fig. 10a. After the MWP is introduced into the model, DTE increases linearly

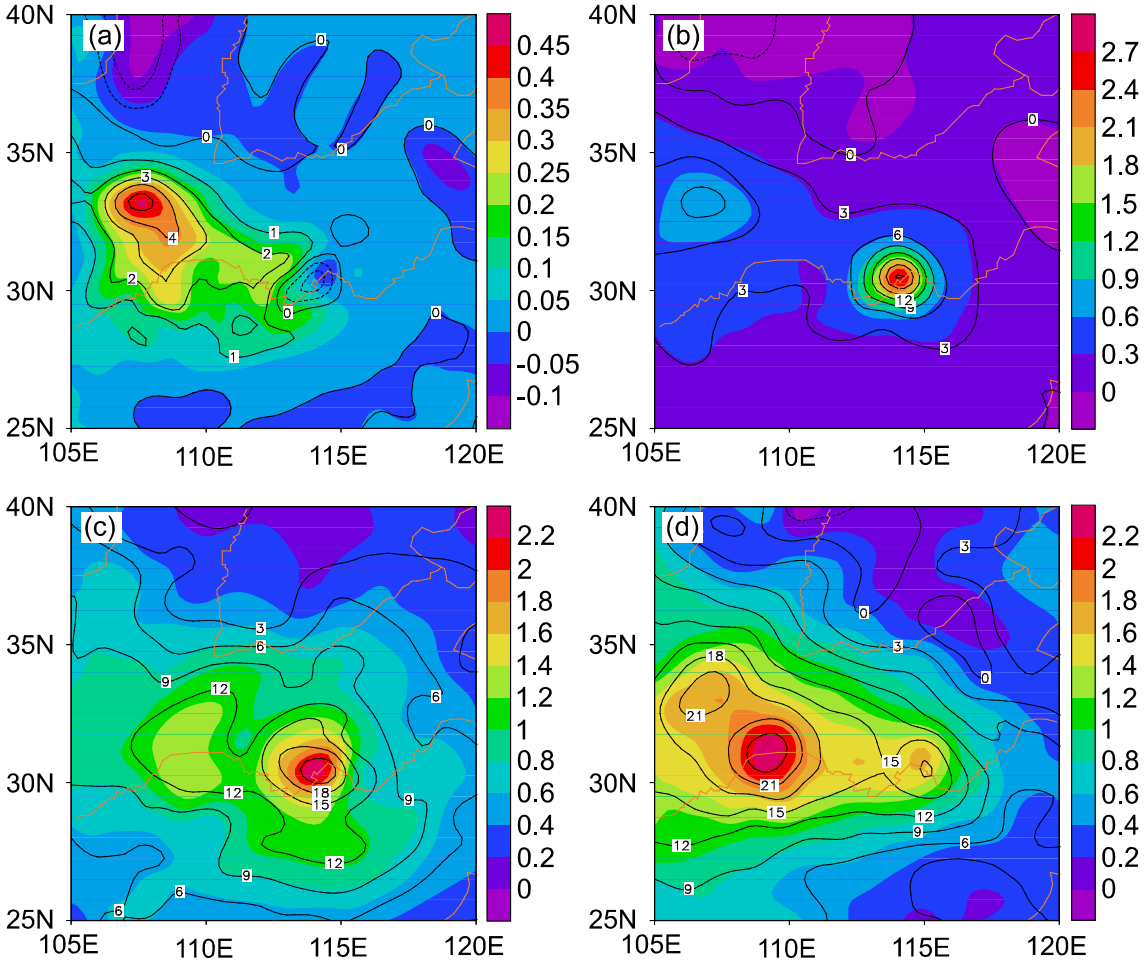

Fig. 8. Horizontal cross section of DDH (lines; contoured every 3 gpm) and DTA (shaded according to scale; units: °C) at (a) t = 18 h, (b) t = 20 h, (c) t = 24 h and (d) t = 30 h.

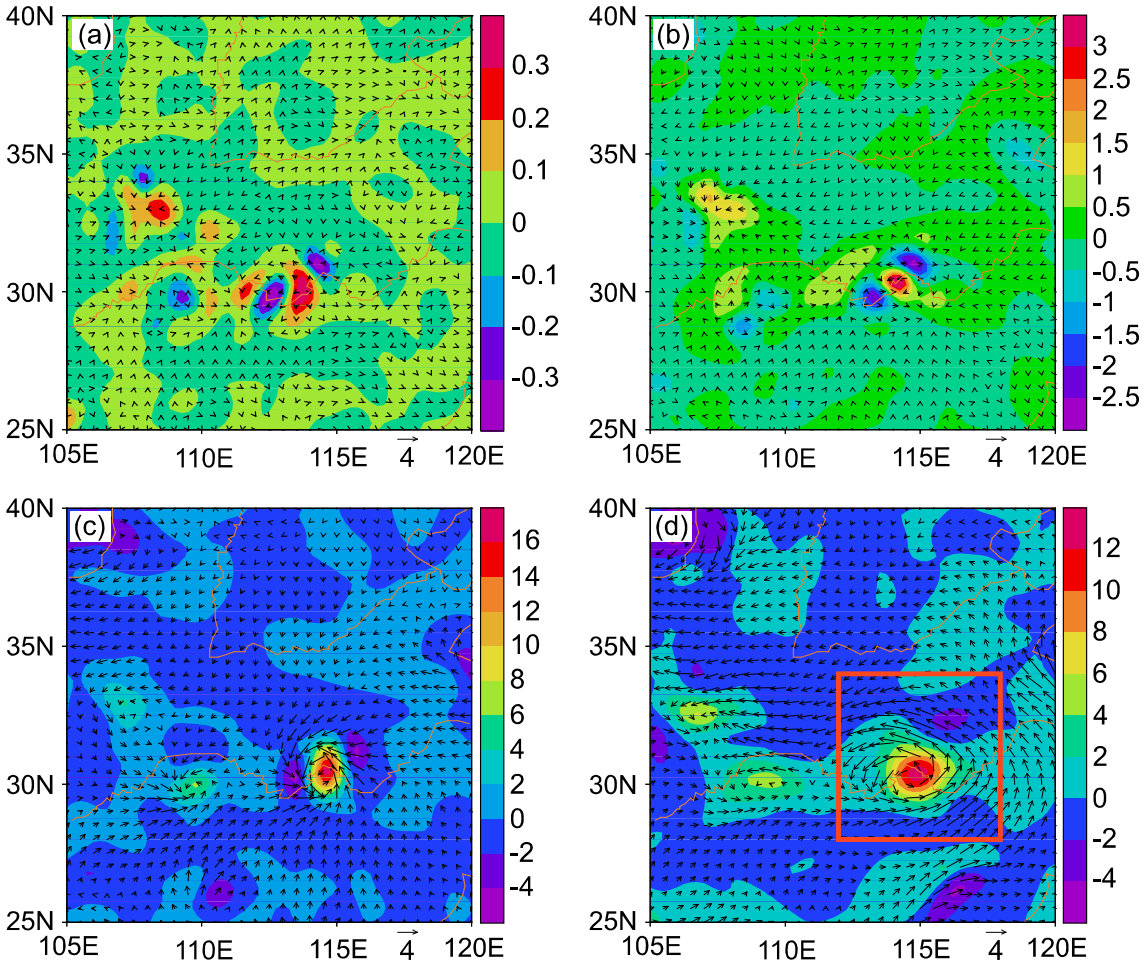

Fig. 9. Horizontal cross section of the difference in vorticity (shaded according to scale; units: $\times 10^{-5}$ s^{-1}) and wind (arrows; units: m s^{-1}) at 700-hPa between EXP2 and EXP1 at (a) t = 18 h, (b) t = 20 h, (c) t = 24 h and (d) t = 30 h. The rectangle denotes the main region of the vortex circulation.

with the integration. However, both TKEs over the same region in EXP1 and EXP2 decrease with the integration (shown in Fig. 10b). This indicates that the decrease of the total energy is compensated by the latent heat energy in EXP2. As some of the latent heat energy is converted into the kinetic energy, the TKE in EXP2 decreases more slowly than that in EXP1.

To reveal the development of the MβV, we calculated the 700-hPa TKE over the MβV circulation field (Fig. 10c). The TKE varies little in EXP1, whereas in EXP2 the TKE increases linearly after t = 18 h. Consequently, the LHF plays an important role in the evolution of the dynamic fields and the development of the MβV.

4. Impacts of moist process on the mLLJ and MβV

Numerical simulations of the mei-yu system conducted by Hsu and Sun (1994) showed that the LHR by stratiform precipitation causes the 850-hPa pressure trough to deepen, which induces convergent motion at low levels and generates a direct, cross-frontal secondary circulation that helps keep the low-level wind supergeostrophic. Using Ertel's PV (e.g., Hoskins et al., 1985) inversion technique (Davis and Emanuel, 1991), Chen et al. (2006) studied an MCS that formed within the mei-yu frontal cloud band. They showed that the latent heating from the MCS generated a positive PV and height fall at low levels. The enhanced height gradient induced northwestward-directed ageostrophic winds and the LLJ formed southeast of the MCS under the effect of Coriolis torque. In this study, we found that the mLLJ to the southwest of the vortex intensifies with the rainfall and the latent heat. It is necessary to analyze the formation mechanism of the mLLJ and mesoscale vortex in more detail.

Figure 11 shows the vertical cross section of temperature departures from the standard temperature of a reference atmosphere along 30.5°N in EXP2. A cold region is evident above grid point (30.5°N, 114°E) at t = 17 h, with the cold center at 770 hPa (Fig. 11a). The low-level air is warmed by the latent heat after the onset of rainfall. A warm center occurs at 900 hPa at t = 18 h (not shown), and it rises to 770 hPa at t = 19 h (Fig. 11b), and to 600 hPa at t = 20 h (not shown). These results demonstrate that the latent heat warms

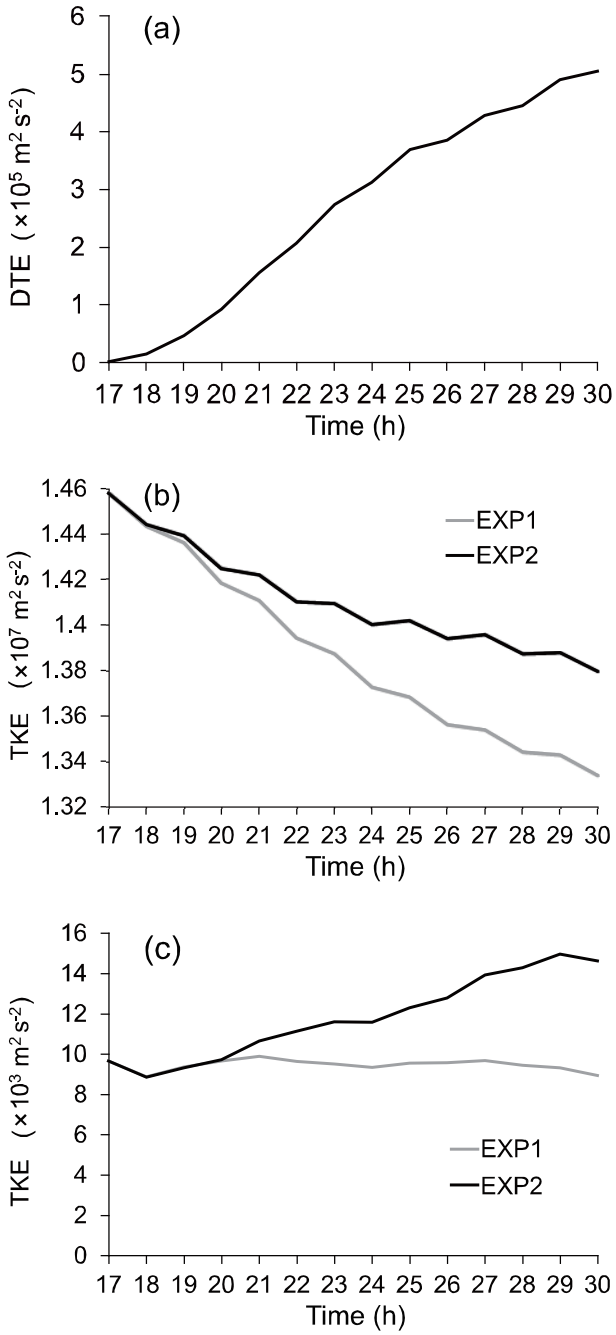

Fig. 10. (a) Evolution of DTE (units: $m^2\ s^{-2}$). Evolution of TKE (units: $m^2\ s^{-2}$) in EXP1 and EXP2 over (b) the same region as the DTE computation region, and (c) the MβV circulation field as shown in Fig. 9d.

the air from low to middle levels. According to the evolution of precipitation intensity within (30°–31°N, 113.5°–114.5°E) shown in Fig. 3, the rainfall is relatively weak at t = 18 h and the convection is initiated at low-levels. When the convection develops upwards, the rainfall intensifies rapidly and the latent heat is released in the middle-to-upper levels. The warm center disappears as the rainfall weakens quickly.

The impact of LHF on the winds is essential for the formation of the mLLJ. Figure 12 shows the evolution of the 850-hPa winds, temperature, and associated 1-h accumulated precipitation in EXP2. A cold center is located to the north of Wuhan with a minimum temperature lower than 21°C, and a prevailing southwesterly wind across most areas to the south of 32°N at t = 17 h (Fig. 12a). With the intensification of rainfall, a warm center forms to the south of Wuhan with a maximum temperature and precipitation intensity greater than 23.5°C and 7 mm h^{-1}, respectively, at t = 18 h (not shown). When the rainfall intensifies to more than 10 mm h^{-1} at t = 19 h, wind convergence occurs in the area surrounding the intense rainfall (Fig. 12b). The convergence is clear at t = 21 h when the precipitation intensity is greater than 40 mm h^{-1} (Fig. 12c). The southwesterly blowing to the south of the intense rainfall region is accelerated by the ageostrophic winds induced by the LHR. However, the 850-hPa temperature near the intense rainfall region decreases to about 21.5°C at t = 21 h, indicating that convection has developed in the upper to middle levels, and rainfall evaporation has cooled the low-level air. By t = 23 h, a cold center forms near Wuhan (Fig. 12d).

The 500-hPa winds and temperature show a similar warm center (not shown), but the warm center occurs at t = 20 h when the maximum 1-h accumulated precipitation was greater than 40 mm; that is, the convection develops leading up to the mature stage, with the main LHR occurring at middle levels. During this stage, the precipitation center is consistent with the 500-hPa warm and divergence centers, and the latent heating induces a divergent ageostrophic wind. This middle-to-upper-level pumping effect favors the intensification of the rainfall.

Figure 13 shows the geopotential height and winds at 850 and 500 hPa in EXP2. At t = 17 h, southwesterlies occur near Wuhan at both 850 and 500 hPa. When the rainfall intensifies at t = 20 h, a meso-low and a meso-high form at 850 hPa and 500 hPa, respectively (Figs. 13a and c). Because of the heavy rainfall, the low-level geopotential heights decrease rapidly, with the minimum value lower than 1400 gpm at t = 20 h. The release of latent heat causes intense convergence to form at low levels, and rotating winds to form near Wuhan under the effect of Coriolis torque. The mLLJ to the southeast of the vortex is formed by the ageostrophic southwesterly winds, and the meso-low with an intense height gradient also forms through the geostrophic adjustment process. The increase in the 500-hPa geopotential height leads to the stretching of the air column and, because of the effects of PV conservation, the intensification of the vorticity.

5. Summary and discussion

This paper describes the use of an improved version of a three-dimensional η-coordinate mesoscale model to numerically simulate the "98.7" heavy rainfall event that occurred on 21 and 22 July 1998 over eastern Hubei Province, China. The high temporal and spatial resolution model output data that show the intense heavy rainfall, col field, MβV, and mLLJ were analyzed. Two experiments were designed, in one of which the LHF scheme was switched off, and in the other

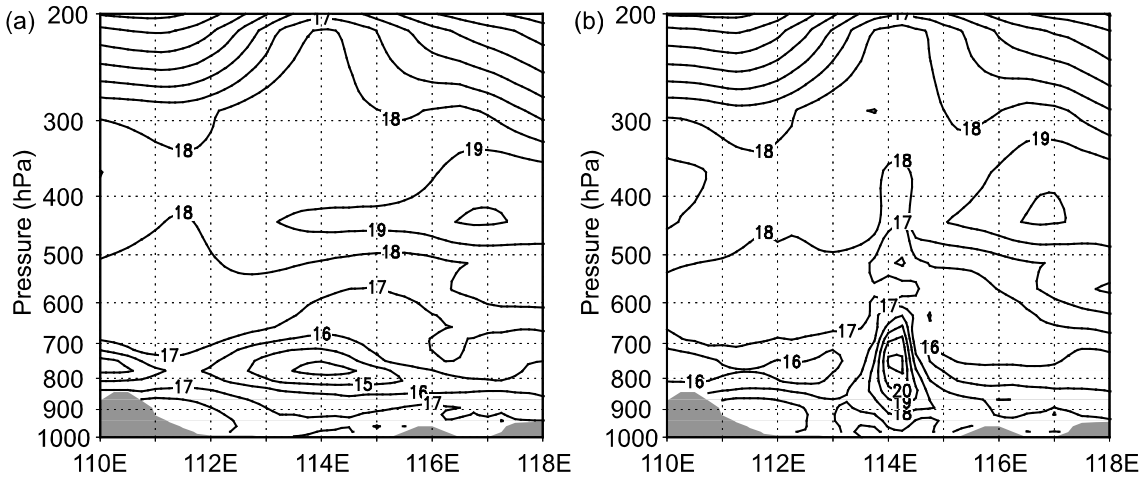

Fig. 11. Vertical cross section of temperature (units: °C) departures from the standard temperature of a reference atmosphere along the latitude of 30.5°N at (a) t = 17 h and (b) t = 19 h in EXP2. The shading shows the topography.

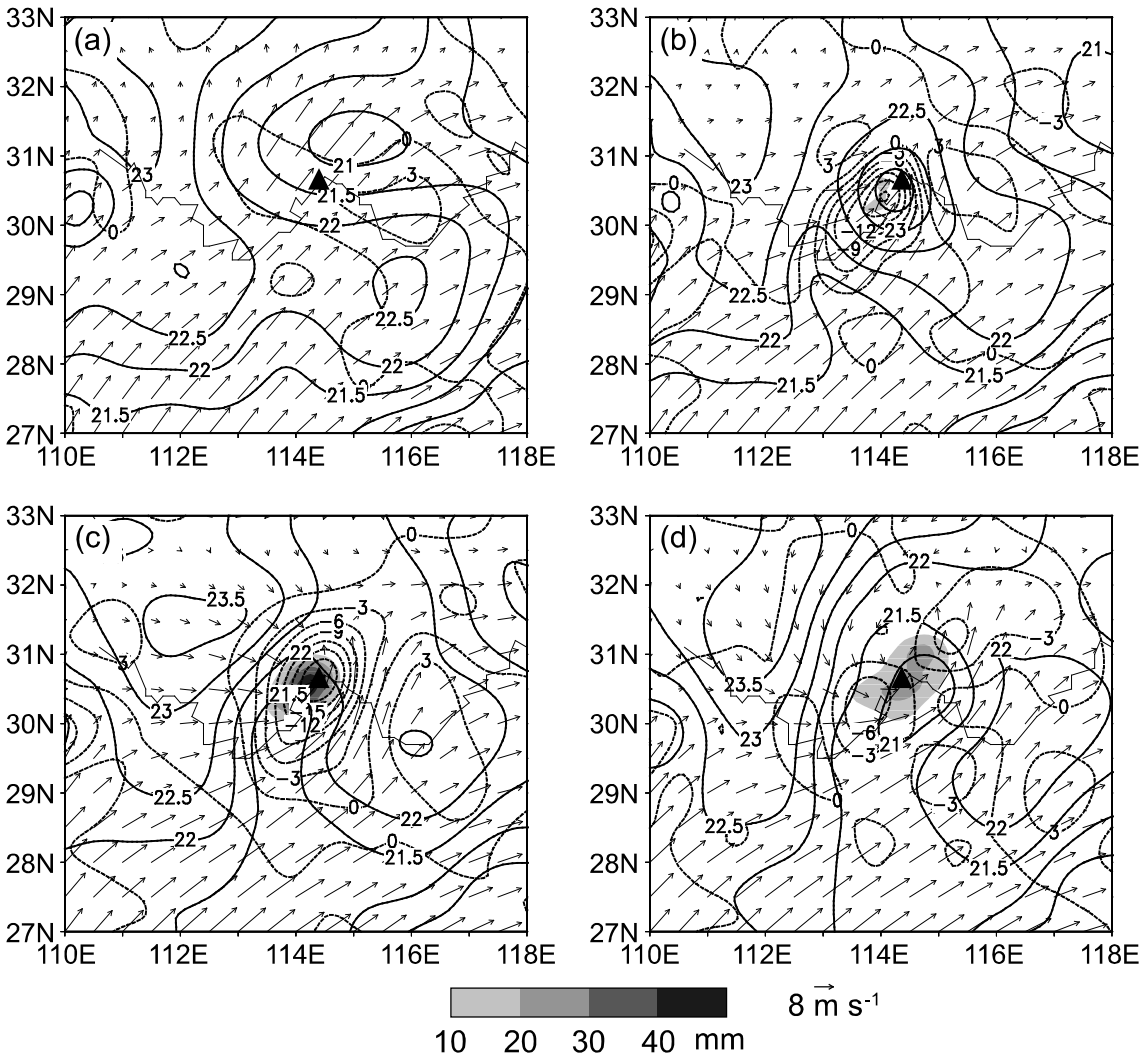

Fig. 12. 850-hPa winds (vectors; units: m s^{-1}), temperature (solid lines; contoured every 0.5°C), divergence (dashed lines; contoured every 3×10^{-5} s^{-1}), and associated 1-h accumulated precipitation (shaded according to scale; units: mm) at (a) t = 17 h, (b) t = 19 h, (c) t = 21 h and (d) t = 23 h in EXP2. The "▲" symbol marks the location of Wuhan.

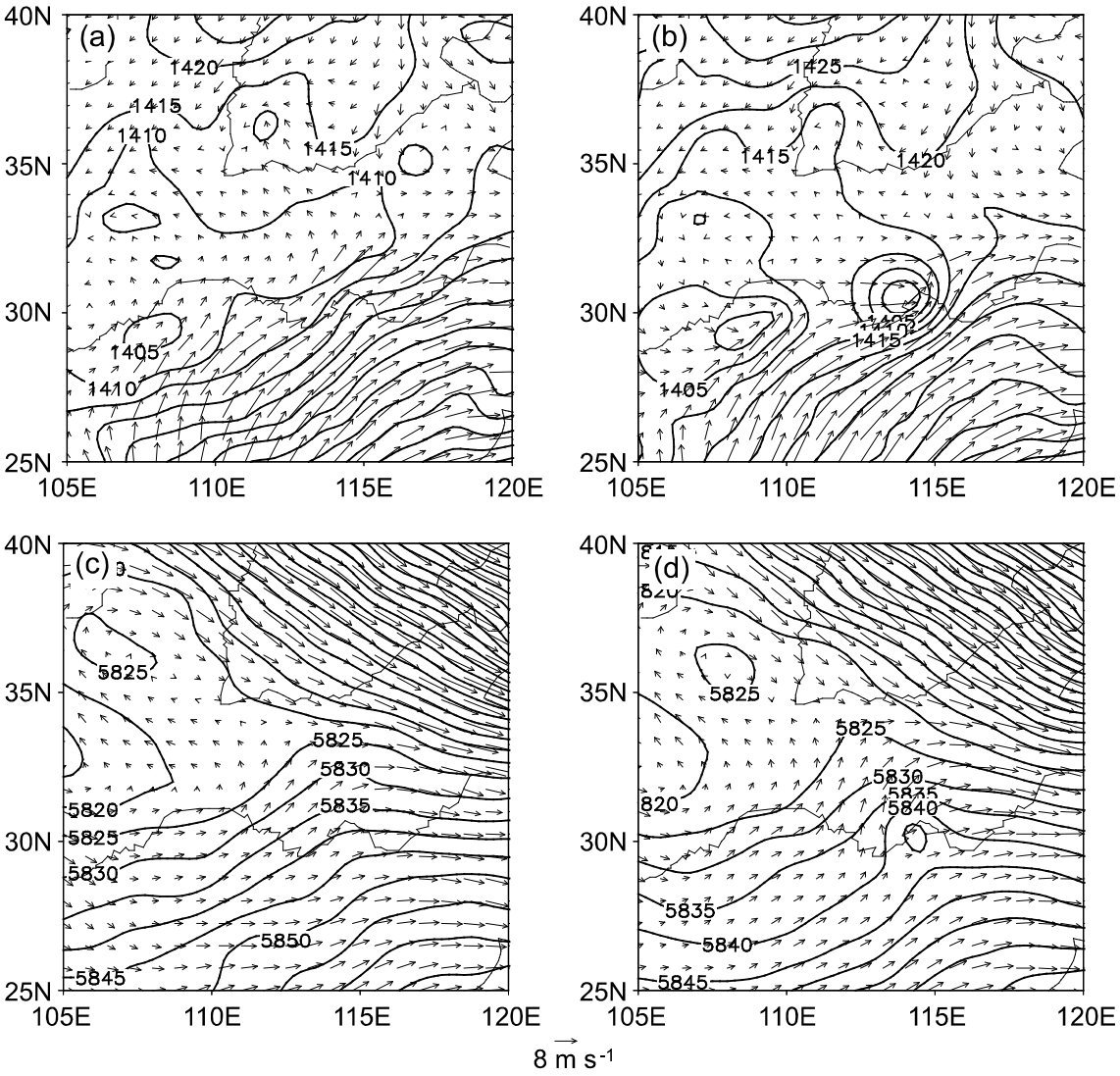

Fig. 13. Geopotential height (lines; contoured every 5 gpm) and winds (arrows units: m s^{-1}) in EXP2 at (a) 850 hPa at t = 17 h, (b) 850 hPa at t = 20 h, (c) 500 hPa at t = 17 h, and (d) 500 hPa at t = 20 h.

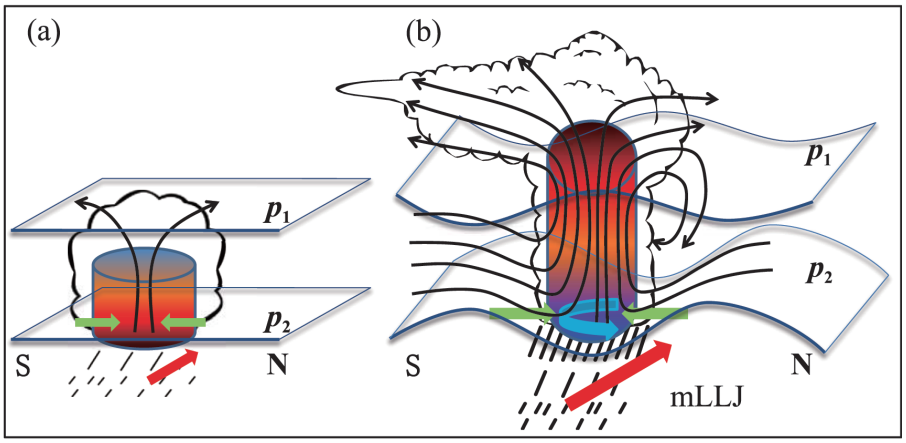

Fig. 14. Schematic representation of the positive feedback among the MβV, rainfall, and mLLJ in the (a) initial stage and (b) mature stage of the MβV. The curved surfaces p_1 and p_2 are the middle- and low-level isobaric surfaces, respectively; the air column color reflects the intensity of latent heating; the red arrows are the mLLJ; the black lines show the air flow in vertical cross section; the green arrows denote convergence; and the blue arrow denotes the cyclonic rotation of the air.

it was switched on after t = 17 h. At t = 17 h, a col field background was evident in the middle reaches of the Yangtze River at low levels, and then an MWP was introduced into the model near the col point to simulate the formation process of the MβV triggered by the MWP.

Our experiments show that the MWPs are able to induce a weak MβV, but the MβV is short-lived and the rainfall is very light without the LHF. When the LHF scheme is switched on as the perturbation is introduced into the model, the MβV develops quickly with intense rainfall and an mLLJ. It is demonstrated that the MβV can be triggered by wind perturbation or an mLLJ in a weak wind environment, and it can develop under the role of LHF. A weak wind environment near the col point and dilatation axis is conducive to the formation of mesoscale vortices.

The DH and TA between 400 and 700 hPa decreased after the MWP was introduced into the model without the LHF. However, they increased rapidly when the LHF scheme was switched on, with the air pressure falling at low levels and rising at upper levels. We found that the MβV, LLJ, and mLLJ have a close relationship with the LHF. The mLLJ must be induced by the ageostrophic winds generated by a local depression in the intense rainfall area. When the convection develops from low levels to upper levels, the rainfall intensifies rapidly and the latent heat is released in the middle-to-upper levels. The release of latent heat causes intense convergence to form at low levels, and rotating winds to form near the area of intense rainfall through Coriolis torque. The mLLJ to the southeast of the vortex is formed by the ageostrophic southwesterly winds, and a meso-low with an intense height gradient also forms, through the geostrophic adjustment process.

Based on our analysis, we developed a conceptual model of the positive feedback among the mesoscale vortex, rainfall, and mLLJ (Fig. 14), which can be summarized as follows: (1) In the initial stage of the MβV (Fig. 14a), the MWP triggers light rainfall in the col field, and latent heating occurs at low levels, leading to weak convergence and ageostrophic winds. (2) In the mature stage of the MβV (Fig. 14b), convection develops into the middle-to-upper levels. The rainfall intensifies as the latent heat warms the middle-to-upper-level air, resulting in an increase in the average temperature and stretching of the air column. Low-level cyclonic circulation forms under the effect of Coriolis torque, and the mLLJ forms to the southeast of the MβV. Then, the strengthened mLLJ leads to the intensification of the vorticity, ascending motion, and rainfall.

Acknowledgements. This research was supported by the National Grand Fundamental Research 973 Program of China (Grant No. 2015CB452800), the National Natural Science Foundation of China (Grant Nos. 41275099, 41205073 and 41275012), and the Natural Science Foundation of the Nanjing Joint Center of Atmospheric Research (Grant No. NJCAR2016MS02). The authors are grateful for the GAME reanalysis data provided by the Japan Meteorological Agency and the Earth Observation Research Center/National Space of Development Agency of Japan.

REFERENCES

Bei, N. F., S. X. Zhao, and S. T. Gao, 2002: Numerical simulation of a heavy rainfall event in China during July 1998. *Meteor. Atmos. Phys.*, **80**, 153–164, https://doi.org/10.1007/s007030200022.

Betts, A. K., 1986: A new convective adjustment scheme. Part I: Observational and theoretical basis. *Quart. J. Roy. Meteor. Soc.*, **112**, 677–691, https://doi.org/10.1002/qj.49711247307.

Chen, Q. S., 1982: The instability of the gravity-inertia wave and its relation to low-level jet and heavy rain. *J. Meteor. Soc. Japan*, **60**, 1041–1057, https://doi.org/10.2151/jmsj1965.60.5_1041.

Chen, G. T. J., C. C. Wang, and L. F. Lin, 2006: A diagnostic study of a retreating Mei-yu front and the accompanying low-level jet formation and intensification. *Mon. Wea. Rev.*, **134**, 874–896, https://doi.org/10.1175/MWR3099.1.

Chen, S. J., Y. H. Kuo, W. Wang, Z. Y. Tao, and B. Cui, 1998: A modeling case study of heavy rainstorms along the Mei-yu front. *Mon. Wea. Rev.*, **126**, 2330–2351, https://doi.org/10.1175/1520-0493(1998)126<2330:AMCSOH>2.0.CO;2.

Cho, H. R., 1993: A mechanism causing mesoscale organizations of precipitation in midlatitude cyclones. *J. Appl. Meteor.*, **32**, 155–160, https://doi.org/10.1175/1520-0450(1993)032<0155:AMCMOO>2.0.CO;2.

Davis, C. A., 1992: A potential-vorticity diagnosis of the importance of initial structure and condensational heating in observed extratropical cyclogenesis. *Mon. Wea. Rev.*, **120**, 2409–2428, https://doi.org/10.1175/1520-0493(1992)120<2409:APVDOT>2.0.CO;2.

Davis, C. A., and K. A. Emanuel, 1991: Potential vorticity diagnostics of cyclogenesis. *Mon. Wea. Rev.*, **119**, 1929–1953, https://doi.org/10.1175/1520-0493(1991)119<1929:PVDOC>2.0.CO;2.

Ding, Y. H., 1992: Summer monsoon rainfalls in China. *J. Meteor. Soc. Japan*, **70**, 373–396, https://doi.org/10.2151/jmsj1965.70.1B_373.

Hoskins, B. J., M. E. McIntyre, and A. W. Robertson, 1985: On the use and significance of isentropic potential vorticity maps. *Quart. J. Roy. Meteor. Soc.*, **111**, 877–946, https://doi.org/10.1002/qj.49711147002.

Hsu, W. R., and W. Y. Sun, 1994: A numerical study of a low-level jet and its accompanying secondary circulation in a Mei-Yu system. *Mon. Wea. Rev.*, **122**, 324–340, https://doi.org/10.1175/1520-0493(1994)122<0324:ANSOAL>2.0.CO;2.

Jiang, Y. Q., and Y. Wang, 2012: Numerical simulation on the formation of mesoscale vortex in col field. *Acta Meteorologica Sinica*, **26**(1), 112–128, https://doi.org/10.1007/s13351-012-0111-6.

Jiang, Y. Q., Y. Wang, and H. Huang, 2012: A study on the dynamic mechanism of the formation of mesoscale vortex in col field. *Adv. Atmos. Sci.*, **29**(6), 1215–1226, https://doi.org/10.1007/s00376-012-1186-9.

Kuo, Y.-H., and R. J. Reed, 1988: Numerical simulation of an explosively deepening cyclone in the eastern Pacific. *Mon. Wea. Rev.*, **116**, 2081–2105, https://doi.org/10.1175/1520-0493(1988)116<2081:NSOAED>2.0.CO;2.

Matsumoto, S., S. Yoshizumi, and M. Takeuchi, 1970: On the structure of the "Baiu Front" and the associated intermediate-scale disturbances in the lower atmosphere. *J. Meteor. Soc. Japan*, **48**, 479–491, https://doi.org/10.2151/jmsj1965.48.6_479.

Ninomiya, K., and T. Akiyama, 1974: Band structure of mesoscale echo clusters associated with low-level jet stream. *J. Meteor. Soc. Japan*, **52**, 300–313, https://doi.org/10.2151/jmsj1965.52.3_300.

Ninomiya, K., 2000: Large- and meso-α-scale characteristics of Meiyu/Baiu front associated with intense rainfalls in 1-10 July 1991. *J. Meteor. Soc. Japan*, **78**, 141–157, https://doi.org/10.2151/jmsj1965.78.2_141.

Novak, D. R., B. A. Colle, and R. McTaggart-Cowan, 2009: The role of moist processes in the formation and evolution of mesoscale snowbands within the comma head of Northeast U. S. cyclones. *Mon. Wea. Rev*., **137**, 2662–2686, https://doi.org/10.1175/2009MWR2874.1.

Posselt, D. J., and J. E. Martin, 2004: The effect of latent heat release on the evolution of a warm occluded thermal structure. *Mon. Wea. Rev*., **132**, 578–599, https://doi.org/10.1175/1520-0493(2004)132<0578:TEOLHR>2.0.CO;2.

Stoelinga, M. T., 1996: A potential vorticity–based study of the role of diabatic heating and friction in a numerically simulated baroclinic cyclone. *Mon. Wea. Rev*., **124**, 849–874, https://doi.org/10.1175/1520-0493(1996)124<0849:APVBSO>2.0.CO;2.

Tan, Z. M., F. Q. Zhang, R. Rotunno, and C. Snyder, 2004: Mesoscale predictability of moist baroclinic waves: Experiments with parameterized convection. *J. Atmos. Sci*., **61**, 1794–1804, https://doi.org/10.1175/1520-0469(2004)061<1794:MPOMBW>2.0.CO;2.

Uccellini, L. W., R. A. Petersen, P. J. Kocin, K. F. Brill, and J. J. Tuccillo, 1987: Synergistic interactions between an upper-level jet streak and diabatic processes that influence the development of a low-level jet and a secondary coastal cyclone. *Mon. Wea. Rev.*, **115**, 2227–2261, https://doi.org/10.1175/1520-0493(1987)115<2227:SIBAUL>2.0.CO;2.

Wang, Z., G. Q. Zhai, and K. Gao, 2003: Analysis and numerical simulation of a meso-β-scale vortex in the middle reaches of the Yangtze River. *Acta Meteorologica Sinica*, **61**, 66–77, https://doi.org/10.11676/qxxb2003.007. (in Chinese with English abstract)

Xu, W. H., Y. Q. Ni, X. K. Wang, X. X. Qiu, X. H. Bao, and W. Y. Jin, 2011: A study of structure and mechanism of a meso-beta-scale convective vortex and associated heavy rainfall in the Dabie mountain area part I: Diagnostic analysis of the structure. *Adv. Atmos. Sci*., **28**(5), 1159–1176, https://doi.org/10.1007/s00376-010-0170-5.

Yu, R. C., Q. C. Zeng, G. K. Peng, and F. X. Chai, 1994: Research on "Ya-An-Tian-Lou". Part II: Numerical trial-forecasting. *Scientia Atmospherica Sinica*, **18**(5), 535–551, https://doi.org/10.3878/j.issn.1006-9895.1994.05.04. (in Chinese with English abstract)

Zhang, D. L., and R. A. Anthes, 1982: A high-resolution model of the planetary boundary layer-sensitivity tests and comparisons with SESAME-79 data. *J. Appl. Meteor*., **21**, 1594–1609, https://doi.org/10.1175/1520-0450(1982)021<1594:AHRMOT>2.0.CO;2.

Zhang, F., C. Snyder, and R. Rotunno, 2003a: Effects of moist convection on mesoscale predictability. *J. Atmos. Sci*., **60**, 1173–1185, https://doi.org/10.1175/1520-0469(2003)060<1173:EOMCOM>2.0.CO;2.

Zhang, Q. H., K. H. Lau, Y. H. Kuo, and S. J. Chen, 2003b: A numerical study of a mesoscale convective system over the Taiwan Strait. *Mon. Wea. Rev*., **131**, 1150–1170, https://doi.org/10.1175/1520-0493(2003)131<1150:ANSOAM>2.0.CO;2.